Acquiring rotation data on the ocean bottom without rotation sensors

Ohad Barak, Kerry Key, Steven Constable, Paul Milligan and Shuki Ronen

ABSTRACT

There are currently no widely available rotation sensors that can operate on the ocean-bottom. We derive rotation data on the ocean bottom from two surveys that were not originally designed to record them: 1) from geophone recordings in the Moere Vest ocean-bottom survey by differencing adjacent geophones; and 2) from magnetometer recordings in the SERPENT CSEM ocean-bottom survey by extrapolating from the deviations in magnetic field projections on the magnetometer components.

INTRODUCTION

Rigid bodies in a three dimensional world have six degrees of freedom: three components of translation and three components of rotation. The time derivatives of translations are the particle velocities and the rotations are the pitch, roll and yaw, as shown in the following table:

Axis	Translation		Rotation	
Z	Vertical	v_z	Yaw	r_z
X	Radial	v_x	Roll	r_x
Y	Transverse	v_y	Pitch	r_y

where v_i are particle velocities along the i axis, and r_i are rotation rates around the i axis.

In ocean-bottom node acquisition, multicomponent geophones that are coupled to the seafloor record the vertical and the two horizontal components of particle velocity $\vec{v}$. Additionally, a hydrophone records the divergence of the translation wavefield $P = \kappa\,(\nabla \cdot \vec{u})$, where $\vec{u}$ are particle displacements and κ is the bulk modulus of the water to which the hydrophones are coupled. Rotation rates are a measurement of the curl of the particle velocity wavefield $\vec{r} = \frac{1}{2}(\nabla \times \vec{v})$, and are a recording of the anti-symmetric strains of the medium (Cochard et al., 2006).

Vassallo et al. (2012) use hydrophones together with pressure gradient sensors in marine streamer acquisition to interpolate the pressure wavefield in the crossline direction, between streamer cables. Similarly, the rotational components can be used

to interpolate vertical geophone data (Edme et al., 2014), and spatial aliasing of high-wavenumber arrivals can thus be mitigated. Barak et al. (2014b) show that rotation data are extra information, are independent of geophone data, and can be used in conjunction with geophone data to identify and separate wave-modes on land using singular-value decomposition polarization analysis.

As of yet there are no industry-grade solutions for recording rotational motion on the ocean bottom, though a few such recording stations have been deployed previously by Pillet et al. (2009). The objective of this paper is to show how rotation data can be extracted from existing ocean-bottom recordings.

THE MOERE VEST OCEAN-BOTTOM SURVEY

The Moere Vest data include a group of 26 four-component ocean-bottom nodes, a "microspread," which have a unique geometry in that they are spaced at 2 m intervals. We estimated the three-component rotational motion by differencing adjacent geophones of these microspread nodes. Geophone differencing as a method of estimating rotational motion has been shown previously in Muyzert et al. (2012) and Barak et al. (2014a). In the case of the microspread, the short 2 m interval between receivers ensures that most of the data are sampled well enough to prevent spatial aliasing. Therefore, we assume that a differencing of the data recorded by adjacent nodes pertains to differences of displacements within half a wavelength.

Though the acquired data may be of high quality, any differencing of data coming from physically separate sensors must be done with the caveat that we are in effect decreasing the signal to noise ratio in the resulting differenced data. Each sensor may have a slightly different coupling to the medium, reducing the reliability of the difference signal. Also, the data and the data-difference are not collocated in space. The proper way of obtaining a recording of any physical quantity is to design a sensor that can measure that particular quantity directly at one point in space. The resulting rotation data we get from differencing are an estimate of the data which would have been recorded with rotation sensors. We are able to obtain this estimate due to the special geometry of the microspread.

Estimating rotational motion from geophone data

The stress-displacement relation for tangential stresses reads:

$$\sigma_{ij} = \mu \left(\partial_j u_i + \partial_i u_j \right), \tag{1}$$

where σ_{ij} are the tangential stresses, u_i are particle displacements and μ is the shear modulus.

At a free surface, or at an interface between a medium with shear strength and one without shear strength (such as the ocean-bottom interface), the tangential stresses

σ_{ij} are zero. Therefore, assuming we have receivers laid out on a flat, horizontal sea bottom, we have

$$\begin{aligned} \partial_z u_y &= -\partial_y u_z, \\ \partial_z u_x &= -\partial_x u_z, \end{aligned} \tag{2}$$

meaning that the vertical derivative of the horizontal displacement component is equal to the horizontal derivative of the vertical displacement component.

Rotation is defined as the curl of the wavefield. Since our geophones record the time derivative of displacement (particle velocity), we use the time derivative of rotation, or rotation rate:

$$\begin{aligned} \vec{r} = \frac{1}{2}(\nabla \times \vec{v}) &= \hat{X}\left(\partial_y v_z - \partial_z v_y\right)/2 \\ &+ \hat{Y}\left(\partial_z v_x - \partial_x v_z\right)/2 \\ &+ \hat{Z}\left(\partial_x v_y - \partial_y v_x\right)/2, \end{aligned} \tag{3}$$

where $\hat{X}$, $\hat{Y}$ and $\hat{Z}$ are the rotation axes. Substituting equation 2 into 3, we see that on the sea bottom

$$r_x = \partial_y v_z, \quad r_y = -\partial_x v_z, \quad r_z = \frac{1}{2}\left(\partial_x v_y - \partial_y v_x\right), \tag{4}$$

i.e., the horizontal rotation-rate components can be derived from the vertical geophones, and the vertical rotation-rate component can be derived from the horizontal geophones.

Microspread geometry

Since we intend to perform geophone differencing, the receiver positions are of high importance. An error in positioning could lead to an error in the derived rotation data. There were two sets of fields in the SEGY files that indicated receiver positions. One of them was the "as-laid" positions, which are the coordinates of the underwater Remotely Operated Vehicle (ROV) that deployed the nodes on the sea bottom. The other set of receiver positions were calculated using the first-break arrival time at each node from all shots in the survey. Figure 1(a) shows these two sets of receiver positions.

Despite the fact that the first-break positions appear too "regular", we opted to use these node positions for the microspread, since we also have video footage of the node deployment showing a very regular geometry. An example is shown in Figure 1(b). The ability of the ROV operator to see all nodes during deployment contributed to the positioning accuracy.

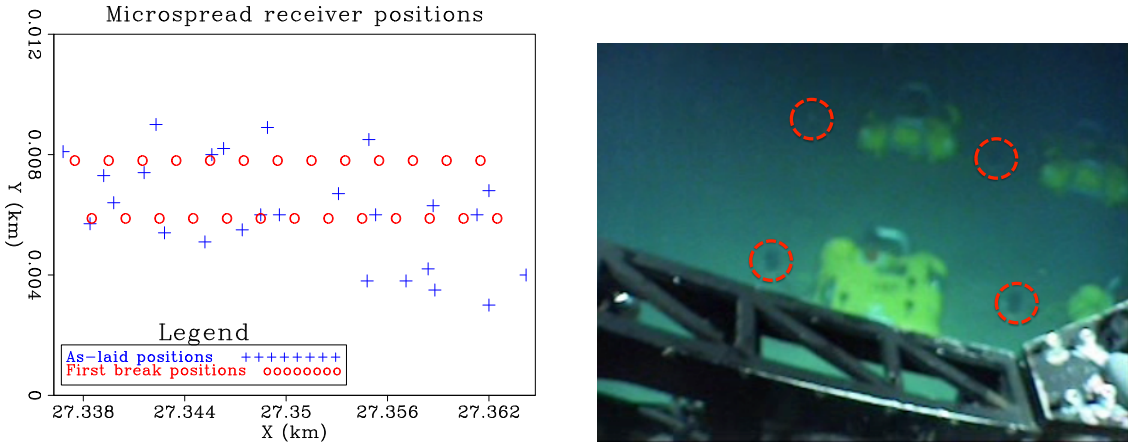

(a) (b)

Figure 1: (a) Microspread receiver "as-laid" positions (blue) vs. first-break positions (red circles). The length of the receiver line is 26 m, and the nominal receiver spacing is 2 m. (b) Photo taken by ROV operator showing four of the ocean-bottom nodes of the microspread. The sensors are indicated by the red circles. Note the regularity of the deployment. [**NR**]

The length of the shot line we used was 55 km, with a shot interval of 50m, traversing almost directly above the nodes of the microspread. The microspread nodes were positioned near the center of the shot line. More than 90% of the shots have less than 5 m of crossline offset. Since the receivers were at a depth of 1.6 km, the data are effectively 2D. We removed the receiver instrument signature and aligned the horizontal geophone components to the 2D survey coordinates.

6-component data from the Moere Vest survey

To generate the three-component rotation-rate data we differenced adjacent receiver stations, effectively executing a finite-difference approximation to equations 4. Figures 2(a), 2(c) and 2(e) are the vertical (v_z), inline (v_x) and crossline (v_y) geophone components of the receiver gather of one node of the microspread. Figures 2(b), 2(d) and 2(f) are the yaw (r_z), roll (r_x) and pitch (r_y) rotational components. Notice that adjacent to each particle velocity component is the rotational component around that geophone's axis.

We are not displaying the direct arrival and some of the associated bubbles that are between $t = 1.08$s and $t = 1.75$s. The water-bottom multiple appears at $t = 3.25$s, and can be seen on the v_z and v_x sections.

The v_z component seems to contain mostly high-frequency reflections with a moveout consistent with P-wave velocity, but there are some lower frequency events that have a much slower moveout. These events are commonly called "Vz noise", and

may be caused by shear-wave scattering in an inhomogeneous seabed, which in turn can generate Scholte waves on the seabed. The v_x component contains mostly those shear-induced events, but some of the P-wave events apparent on v_z are also visible. The v_y component is much weaker than the other two geophone components, but a shear-induced event similar to the one on the v_x component at $t = 3.3$s is prominent. It is possible that the shear energy is indeed coming from shear-wave reflections, however on a receiver gather it is difficult to tell the difference between reflected shear waves and scattered Scholte waves based solely on moveout information.

Observing the rotational components, we see that the one with the greatest energy is r_y. This fits with our expectation. Since the survey geometry is practically 2D, most of the translation should occur in the vertical and inline directions, which means that most of the rotational motion should occur around the crossline direction. Note also the generally increased noise level on the rotational components, which we attribute to the geophone differencing operation.

Compare the v_z and r_y components, and observe how the P-waves are almost not visible on r_y, even though this section was obtained using two adjacent vertical geophones. This indicates that the P-waves generate a similar response on adjacent vertical geophones, and are removed by the differencing. Another way of saying the same thing is that the P-waves do not generate a strong rotational deformation of the surface. Instead, we see a section that is more similar to v_x, with events that have shear-wave moveouts (though slightly delayed compared to v_x). Shear and Scholte waves generate a shear deformation of the surface, which manifests itself as rotational motion. Therefore, rotation data should preferentially record shear waves, and indeed the P events on the r_y component are much weaker than those visible on the v_z and v_x components.

The r_x rotational component seems to also contain some shear-induced events. They are slightly weaker than the events on r_y, indicating that if these are indeed the result of scattered shear waves, then these waves are causing mainly rotation around the crossline axis. The r_z section is the weakest of the rotations (by a factor of 2 compared with r_y). This component should record events that cause a horizontal deformation around the vertical axis. The energy on the r_z component seems to also be related to the shear-induced waves. One explanation could be that multiple scatterings in the near surface are generating horizontal shear deformations of the medium.

THE SERPENT ELECTROMAGNETIC SURVEY

The SERPENT controlled source electromagnetic survey (Key et al., 2012; Naif et al., 2013) took place offshore Nicaragua on May 2010. 55 ocean-bottom EM nodes were deployed along a line perpendicular to a sudbuction zone. Each node had two horizontal induction-coil magnetic field sensors, and two horizontal electric field sensors. A composite node also had a three-component geophone in addition to the EM sensors.

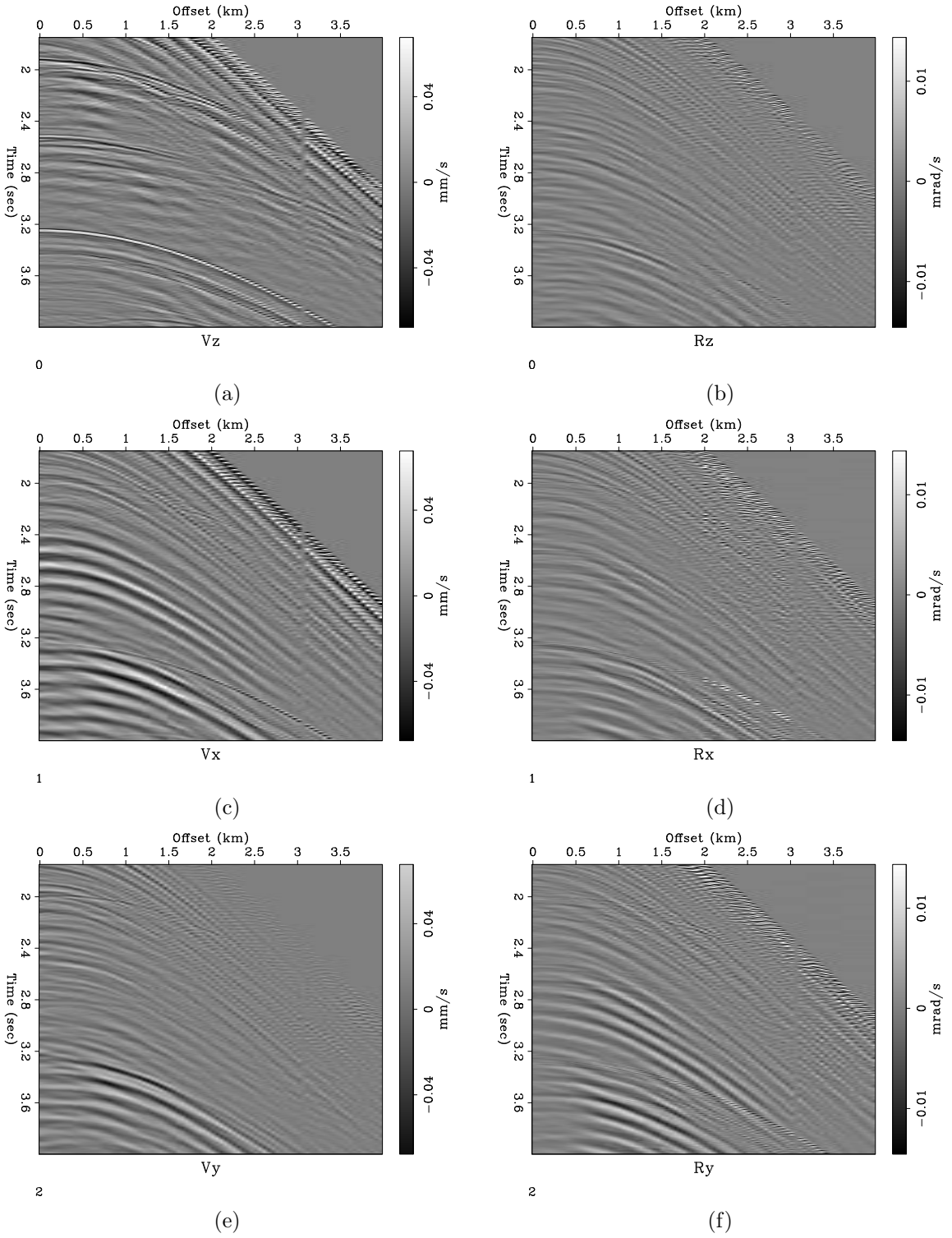

Figure 2: Six-component receiver gather of one node of the microspread of the Moere Vest data. (a) Vertical particle velocity v_z. (b) Yaw rotation r_z. (c) Inline particle velocity v_x. (d) Roll rotation r_x. (e) Crossline particle velocity v_y. (f) Pitch rotation r_y. The rotational components contain mostly the shear-induced energy, and have a lower signal to noise ratio. [**CR**]

Information from the USGS website regarding this earthquake is shown in Figure 3, displaying the earthquake, node line and composite node positions.

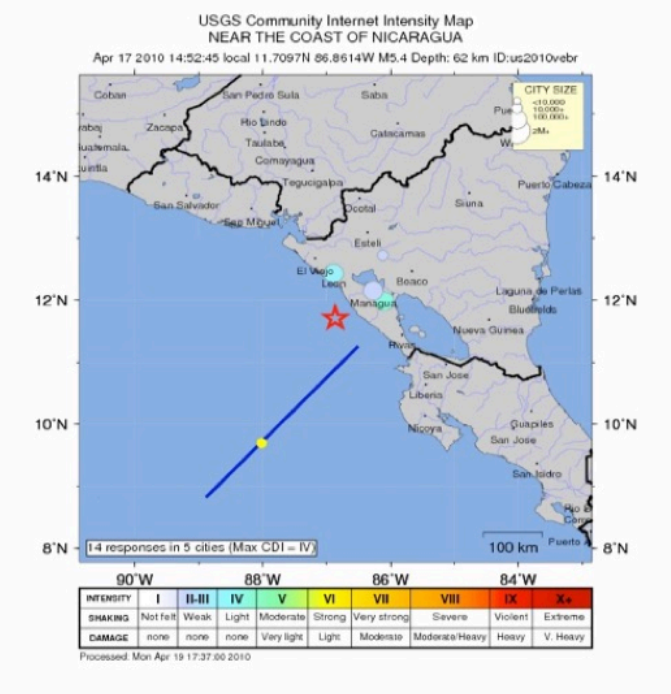

Figure 3: USGS report pertaining to the earthquake (indicated by the red star) that occurred during the SERPENT EM survey. The blue line indicates the EM ocean-bottom node line, where the yellow dot is the position of the composite sensor which had a three-component geophone in addition to the EM sensors. [**NR**]

As expected, the earthquake was recorded on the geophone components of the composite node. The data are shown in Figure 5(a). The P-wave arrives at about $t = 3186.5$s, and the S-wave comes in 2 seconds later. Unexpectedly however, the data of the two magnetic components in Figure 5(b) show a remarkably similar behaviour to the geophone data.

We interpret the magnetic data as resulting from a rotation of the ground caused by the seismic waves generated by the earthquake. The node body is coupled to the seabed via a 150 kg slab of concrete. Therefore, the magnetic sensors in the node body rotate together with the ground. The Earth's magnetic field, however, does not rotate and is effectively constant in direction and in amplitude for the duration of the earthquake. The ground rotation therefore manifests itself as a change in the projection of the Earth's magnetic field on the node's magnetic sensor components. An illustration of this is shown in Figure 4. This concept was explored previously in Kappler et al. (2006) using land data recorded by USGS permanent stations.

From magnetic field projections to ground rotations

After designature, the magnetometer data are in terms of deviation of the magnetic field strength on the two horizontal components over time:

$$\Delta\vec{H}(t) = [\Delta H_x(t), \Delta H_y(t)]. \tag{5}$$

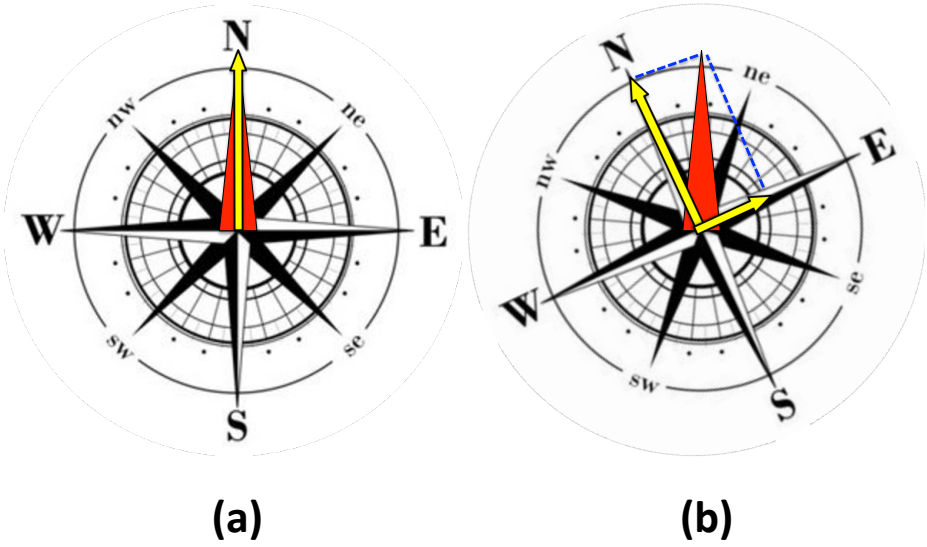

Figure 4: Illustration of how ground rotation is recorded on the magnetic field sensor as represented by the compass, which is coupled to the ground. (a) Before ground rotation, the magnetic field (red) is recorded only by the North component (yellow). (b) During ground rotation, the magnetic field (red) does not change, but its projection on the North and East components (yellow) changes. We can calculate the amount of rotation from the change in projection. Note that translations of the ground will not result in a change of the projection of the magnetic field on the magnetic components. [**NR**]

We deduced the vertical magnetic component by rotating the horizontal node components to geographic North. We then added the ambient magnetic field values for the North and East magnetic components, as given by the British Geological Survey's World Magnetic Model, to the rotated magnetic horizontal components. We then use the total magnetic field strength at the location of the node and at the time of the survey to obtain the vertical magnetic component:

$$H_z(t) = \sqrt{H^2_{\text{total}} - H^2_x(t) - H^2_y(t)}. \tag{6}$$

The angle of rotation between consecutive time steps can now be calculated by

$$\theta(t) = \cos^{-1}\left(\frac{\vec{H}(t+\Delta t)\cdot\vec{H}(t)}{\left|\vec{H}(t+\Delta t)\right|\left|\vec{H}(t)\right|}\right), \tag{7}$$

while the unit vector describing the axis of rotation is

$$\hat{\nu}(t) = \frac{\vec{H}(t)\times\vec{H}(t+\Delta t)}{\left|\vec{H}(t)\times\vec{H}(t+\Delta t)\right|}. \tag{8}$$

In order to have the rotation-rate data in terms of Euler angles in the reference frame of the geophone component axes, we must use a quaternion representation. Our quaternion four-vector system state begins with no rotation, i.e.

$$\mathbf{q}_{t=0} = \begin{pmatrix} q_w \\ q_x \\ q_y \\ q_z \end{pmatrix} = \begin{pmatrix} 1 \\ 0 \\ 0 \\ 0 \end{pmatrix}. \tag{9}$$

We use equations 7 and 8 to get the rotation angle θ and the rotation axis $\vec{u}$, and then we convert to a quaternion representation by

$$\mathbf{p}(t) = \begin{pmatrix} \cos\frac{\theta(t)}{2} \\ u_x(t)\cdot\sin\frac{\theta(t)}{2} \\ u_y(t)\cdot\sin\frac{\theta(t)}{2} \\ u_z(t)\cdot\sin\frac{\theta(t)}{2} \end{pmatrix}. \tag{10}$$

In order to rotate our system from its state at time t to its new state at time $t+\Delta t$, we need to apply quaternion multiplication ($\star$) of the quaternion $\mathbf{q}$ by $\mathbf{p}$:

$$\mathbf{q}(t+\Delta t) = \mathbf{p}(t+\Delta t)\star\mathbf{q}(t) = \left(p_w q_w - \vec{p}\cdot\vec{q},\ p_w\vec{q} + q_w\vec{p} + \vec{p}\times\vec{q}\right). \tag{11}$$

We can now retrieve the change in rotation for every time step in terms of Euler angles around each axis using:

$$\Delta\vec{r}(t) = \begin{pmatrix} \arctan\left(\frac{q_y q_z + q_w q_x}{\frac{1}{2} - \left(q_x^2 + q_y^2\right)}\right) \\ \arcsin\left(-2\left(q_x q_z - q_w q_y\right)\right) \\ \arctan\left(\frac{q_x q_y + q_w q_z}{\frac{1}{2} - \left(q_y^2 + q_z^2\right)}\right) \end{pmatrix}. \tag{12}$$

To get the rotation rate, we must divide $\Delta\vec{r}$ by the time step: $\dot{\vec{r}}(t) = \frac{\Delta\vec{r}}{\Delta t}$

Six-component earthquake data

Figure 5(c) shows the three rotational components as derived from the changes in the projection of the magnetic field on the magnetometer components. The radial geophone component seems to correspond with the rotational pitch components, while the roll and yaw components seem relatively weaker. The ratio between mm/s of particle velocity and mrad/s of rotation rate in these data is approximately 10:1. This is similar to what we see for offsets of a few hundred meters in previous rotational studies done with active land seismic surveys. Additionally, assuming a nominal total magnetic field of 50,000 nT, we expect rotation rates to be on the order of 1 mrad/s for magnetic deviations on the order of 1 nT, as occurs here. However, we do not know if the ground rotation is the only source of the changes in the magnetic field projections in the seismic frequency band. Other effects such as the seismoelectric effect may be occurring in conjunction with the ground rotation and contributing to the recorded changes.

DISCUSSION

In current seismic acquisition, geophones record only the displacements but not rotations. However, with the advent of a new generation of seismic sensors, these physical values will be measurable at each receiver position, providing us with 7-component seismic data: 1 pressure, 3 displacements and 3 rotations. Rotation sensors exist and have seen some very limited use in seismic test surveys on land. On the ocean-bottom though, there are as of yet no industry-grade rotation sensors. We therefore derived the rotational components by alternate means for the datasets mentioned in this paper.

We used the fact that the receivers were deployed with small spacings in the Moere Vest survey to difference their data and estimate the rotational motion that would have been recorded had we instruments that were able to measure these physical variables directly on the ocean-bottom, thereby generating seven-component data. We also derive six-component ocean-bottom earthquake data from a three-component

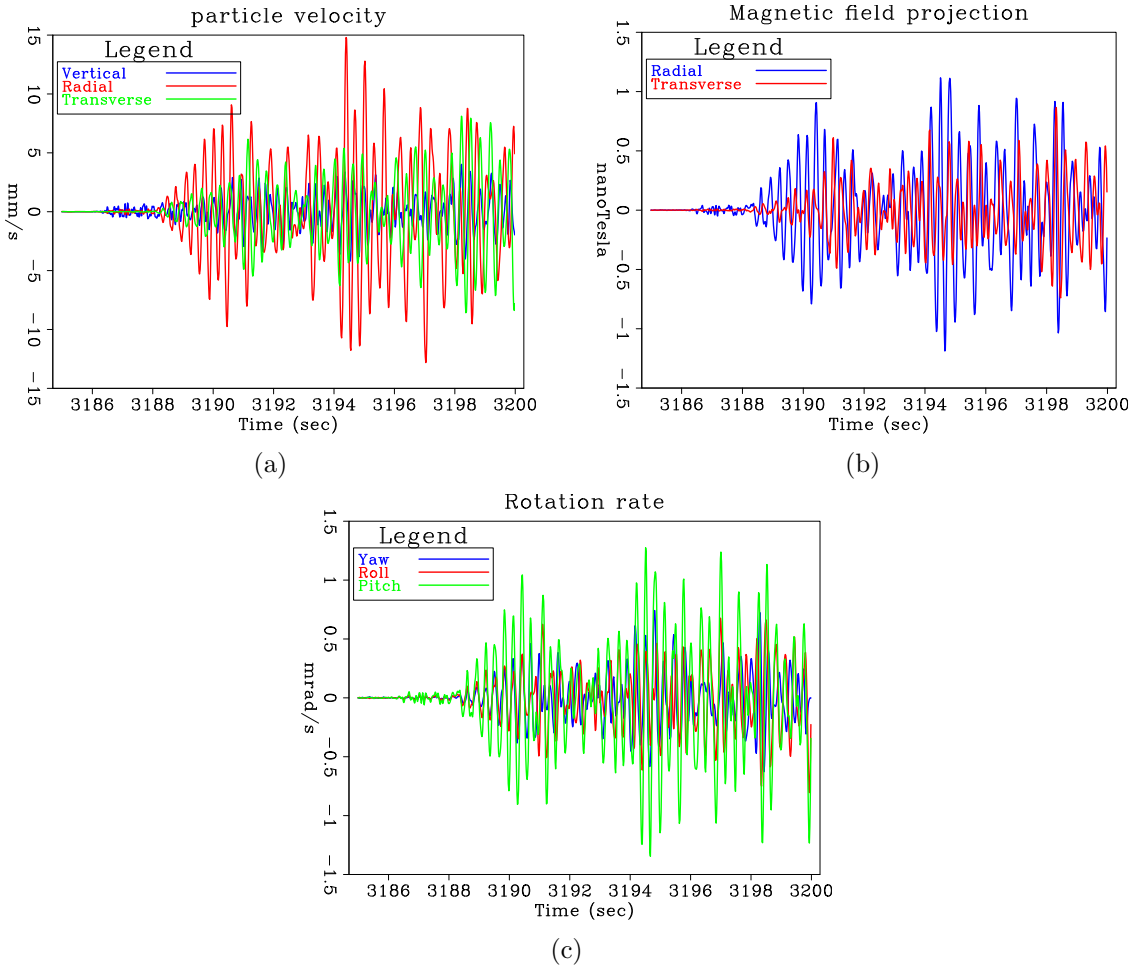

Figure 5: Data of the first 14 second of the earthquake that occurred during the SERPENT survey. Horizontal component data are rotated to minimize the energy on the geophone transverse component. (a) Particle velocity recorded by 3C geophone. (b) Deviations in projection of magnetic field on 2C horizontal magnetometer components. (c) 3 components of rotation rate derived from the 2C magnetometer data. Note the strong amplitudes of the radial geophone component and how there is some correspondence between it and the pitch rotational component. [**ER**]

seismometer and a two-component horizontal magnetometer deployed for the SERPENT CSEM survey.

Both methods we show have possible sources of error in the derived rotation data, and without proper experimentation there is, in principle, no way to validate them. We intend to conduct a land experiment to confirm the derivation of rotations from magnetometer recordings. The experiment will take place in the Mojave desert in California, and will include 3-component rotation sensors, 3-component magnetometers and vertical geophones. We will compare the rotation data as derived from the magnetometers to the rotation data recorded by the rotation sensors. If successful, we may tentatively envision future 7-component seismic acquisition comprising hydrophones, geophones and magnetometers.

ACKNOWLEDGEMENTS

We thank the sponsors of the Stanford Exploration Project, the Seafloor Electromagnetic Methods Consortium, and Seabed Geosolutions for releasing the Moere Vest data. We also thank Robert Brune for many fruitful discussions. The SERPENT project was funded by National Science Foundation grant OCE-0841114.

REFERENCES

Barak, O., S. de Ridder, J. Giles, P. Jaiswal, R. Brune, and S. Ronen, 2014a, Six-component seismic land data acquired with geophones and rotation sensors: Wave-mode separation using 6C SVD: SEG Technical Program Expanded Abstracts, 1863–1867.

Barak, O., F. Herkenhoff, R. Dash, P. Jaiswal, J. Giles, S. de Ridder, R. Brune, and S. Ronen, 2014b, Six-component seismic land data acquired with geophones and rotation sensors: Wave-mode selectivity by application of multicomponent polarization filtering: The Leading Edge, **33**, 1224–1232.

Cochard, A., H. Igel, B. Schuberth, W. Suryanto, A. Velikoseltsev, U. Schreiber, J. Wasserman, F. Scherbaum, and D. Vollmer, 2006, Rotational motions in seismology: Theory, observations, simulation: Earthquake Source Asymmetry, Structural Media and Rotation Effects, 391–411.

Edme, P., E. Muyzert, and E. Kragh, 2014, Efficient land seismic acquisition sampling using rotational data: 76th EAGE Conference and Exhibition, Seismic Noise Attenuation Session, **ELI1 08**.

Kappler, K., N. Cuevas, and J. W. Rector, 2006, Response of induction coil magnetometers to perturbations in orientation: SEG Technical Program Expanded Abstracts, 899–903.

Key, K., S. Constable, T. Matsuno, R. L. Evans, and D. Myer, 2012, Electromagnetic detection of plate hydration due to bending faults at the middle america trench: Earth and Planetary Science Letters, **351**, 45–53.

Muyzert, E., A. Kashubin, E. Kragh, and P. Edme, 2012, Land seismic data acquisition using rotation sensors: 74th Conference and Exhibition, EAGE, Extended Abstracts.

Naif, S., K. Key, S. Constable, and R. L. Evans, 2013, Melt-rich channel observed at the lithosphere-asthenosphere boundary: Nature, **495**, 356–359.

Pillet, R., A. Deschamps, D. Legrand, J. Virieux, N. Bethoux, and B. Yates, 2009, Interpretation of broadband ocean-bottom seismometer horizontal data seismic background noise: Bulletin of the Seismological Society of America, **99**, 1333–1342.

Vassallo, M., K. Eggenberger, D. J. van Manen, K. Ozdemir, J. Robertsson, and A. Ozbek, 2012, Contributions of the horizontal and vertical components of particle velocity in 3D pressure wavefield reconstruction on dense receiver grids using generalized matching pursuit: SEG Technical Program Expanded Abstracts, 1–5.